J. Fluid Mech. (2010), *vol.* 642, *pp.* 373–394.
doi:10.1017/S0022112009991807

Is grid turbulence Saffman turbulence?

P.-Å. KROGSTAD[1]† AND P. A. DAVIDSON[2]

[1]Norwegian University of Science and Technology, N-7491 Trondheim, Norway
[2]University of Cambridge, Cambridge CB2 1PZ, UK

(Received 20 February 2009; revised 27 August 2009; accepted 27 August 2009;
first published online 11 December 2009)

There has been a longstanding debate as to whether the large scales in grid turbulence should be classified as of the Batchelor or Saffman type. In the former, the integral scales, u and ℓ, satisfy $u^2\ell^5 \approx constant$, while in Saffman turbulence we have $u^2\ell^3 = constant$. For strictly homogeneous turbulence the energy decay rates in these two types of turbulence differ, with $u^2 \sim t^{-10/7}$ in Batchelor turbulence and $u^2 \sim t^{-6/5}$ in Saffman turbulence. We present high-resolution measurements of grid turbulence taken in a large wind tunnel. The particularly large test section allows us to measure energy decay exponents with high accuracy. We find that the turbulence behind the grid is almost certainly of the Saffman type, with $u^2\ell^3 = constant$. The measured energy decay exponent, however, is found to lie slightly below the theoretical prediction of $u^2 \sim t^{-1.2}$. Rather we find $u^2 \sim t^{-n}$, with $n = 1.13 \pm 0.02$. This discrepancy is shown to arise from a weak temporal decay of the dimensionless energy dissipation coefficient, $\epsilon\ell/u^3$, which is normally taken to be constant in strictly homogeneous turbulence, but which varies very slowly in grid turbulence.

Key words: homogeneous, theory

1. Introduction

We consider the decay of high Reynolds number isotropic turbulence, as approximated by grid turbulence. In particular, we are interested in the rate of decay of the turbulent kinetic energy, $\langle \mathbf{u}^2 \rangle/2$, and the rate of growth of the integral scale ℓ. It is generally agreed that both $\langle \mathbf{u}^2 \rangle$ and ℓ evolve according to power laws, and there are two classical predictions. In Kolmogorov's theory of the large scales, based on the conservation of Loitsyansky's integral, we expect

$$\langle \mathbf{u}^2 \rangle \ell^5 = constant. \tag{1.1}$$

This may be combined with the empirical law

$$\frac{\mathrm{d}u^2}{\mathrm{d}t} = -A\frac{u^3}{\ell}, \quad A = constant, \tag{1.2}$$

where $u^2 = \langle \mathbf{u}^2 \rangle/3$, to give,

$$\langle \mathbf{u}^2 \rangle \sim t^{-10/7}, \tag{1.3}$$

$$\ell \sim t^{2/7}. \tag{1.4}$$

A competing theory, due to Saffman (1967), has

$$\langle \mathbf{u}^2 \rangle \ell^3 = constant, \tag{1.5}$$

† Email address for correspondence: per.a.krogstad@ntnu.no

which, when combined with (1.2), demands,

$$\langle \mathbf{u}^2 \rangle \sim t^{-6/5}, \tag{1.6}$$

$$\ell \sim t^{2/5}. \tag{1.7}$$

(See also Pullin & Saffman 1998 for a discussion of Saffman turbulence.)

Both types of turbulence may be generated, at least approximately, in computer simulations (see e.g. Ishida, Davidson & Kaneda 2006) and the respective decay laws are recovered. However, it remains an open question as to how grid turbulence should behave. It is not even clear that (1.1)–(1.7) represent the only possibilities, or that all types of grids must produce turbulence of the same class. Nevertheless, it is intriguing that the data of Lavoie, Djenedi & Antonia (2007) show decay exponents for $\langle \mathbf{u}^2 \rangle \sim t^{-n}$ which are not too far from, though lower than, the Saffman estimate of $n = 6/5$. Could it be that grid turbulence is Saffman turbulence?

There have been many measurements of decay exponents over the years. Comte-Bellot & Corrsin (1966) found $1.15 < n < 1.29$ and Warhaft & Lumley (1978) estimated $n \sim 1.34$, to mention just a few. In most cases the uncertainty in the determination of the exponent is linked to the unknown virtual origin in time. We investigate this question by performing high spatial resolution experiments in a large wind tunnel. The long test section, which is more than 250 mesh lengths, minimizes the uncertainty in using the data to estimate power-law exponents for $\langle \mathbf{u}^2 \rangle$ and ℓ. As a result we are able to determine the decay exponents to high accuracy. The test section is also wide enough to minimize sidewall effects.

Perhaps it is worthwhile highlighting some of the main findings of the paper. In § 2 we discuss the theoretical decay laws of Kolmogorov and Saffman, as well as possible alternative laws. We show that, provided A in (1.2) is indeed a constant, the Saffman decay exponent of $n = 6/5$ represents a theoretical minimum for n. That is, the turbulence can decay no more slowly than $\langle \mathbf{u}^2 \rangle \sim t^{-1.2}$. However, if A varies slowly with t, as $A \sim t^{-p}$, $p \ll 1$, then the decay exponent for Saffman turbulence changes to $n = 1.2(1 - p)$, which again represents a theoretical minimum decay rate. So the invariance, or otherwise, of A is important.

At first sight it seems odd that A should be considered a (weak) function of t. The usual argument for A being constant is that, in strictly homogeneous turbulence, the dissipation ϵ, which is a surrogate for the flux of energy from the large to small scales, is a function of the large scale quantities $\langle \mathbf{u}^2 \rangle$ and ℓ only. Dimensional analysis then demands, $\epsilon \ell / \langle \mathbf{u}^2 \rangle^{3/2} \sim A = constant$. However, in grid turbulence the streamwise decay of kinetic energy, $\mathrm{d}(\langle \mathbf{u}^2 \rangle/2)/\mathrm{d}x$, means that the turbulence is not strictly homogeneous and we have the possibility that ϵ is now a function of $\langle \mathbf{u}^2 \rangle$, ℓ and $\mathrm{d}(\langle \mathbf{u}^2 \rangle/2)/\mathrm{d}x$, which can be written as $\epsilon = \epsilon(\langle \mathbf{u}^2 \rangle, \ell, \epsilon/U)$, where U is the mean velocity in the tunnel. In dimensionless terms we have

$$\epsilon \ell / \langle \mathbf{u}^2 \rangle^{3/2} \sim F(\langle \mathbf{u}^2 \rangle / U^2), \tag{1.8}$$

or equivalently,

$$A = F(\langle \mathbf{u}^2 \rangle / U^2), \tag{1.9}$$

where F is some unknown function. Thus A could be a weak function of x (or t) in grid turbulence, even if not in strictly homogeneous turbulence.

There is a second reason why we might expect A to vary slowly with x. In the experiment the Reynolds number based on the Taylor microscale, Re_λ, varies along the test section, typically starting at around $Re_\lambda \sim 80$ and then dropping to $Re_\lambda \sim 70$ at the exit of the section (see § 4.1). It is well known that A is a weak function of Re_λ

when $Re_\lambda < 100$, and so this slight variation in Re_λ could manifest itself in a slow evolution in A. In summary, then, A may vary due to weak inhomogeneity or due to a slow decline in Re_λ.

In § 3 we describe the experimental set-up and in § 4 the data is discussed. Our primary finding is that our turbulence is indeed Saffman turbulence, with $\langle \mathbf{u}^2 \rangle \ell^3 = constant$, but that the energy decay exponent lies slightly below the Saffman value of $n = 1.2$. In fact we find $n = 1.13 \pm 0.02$. As suggested above, this discrepancy can be traced back to a slow temporal variation in A, which is found to take the form $A \sim t^{-p}$, $p \approx 0.075$.

2. A review of theoretical decay laws in isotropic turbulence

We now summarize the various decay laws which, on theoretical grounds, one might expect to see in freely decaying isotropic turbulence. These fall into two categories: the classical decay laws of Kolmogorov and Saffman, and the more general cases that arise when we allow for non-analytic behaviour of the spectral tensor (the Fourier transform of the two-point correlation $\langle u_i u'_j \rangle$). Let us start with the classical theories.

2.1. *Classical decay laws*

Consider fully developed isotropic turbulence in which the Reynolds number is high, $Re = u\ell/\nu \gg 1$, so that Kolmogorov's 1941 theory applies. (Here $u = \langle u_x^2 \rangle^{1/2}$ is the usual integral velocity scale and ν the viscosity.) In such a case we expect the large scales of the turbulence to be self-similar when scaled with u and ℓ, and the small scales to be self-similar when scaled using the Kolmogorov microscales, υ and η.

Now the two-point velocity correlation $\langle \mathbf{u} \cdot \mathbf{u}' \rangle(r)$ is related to the energy spectrum $E(k)$ by

$$E(k) = \frac{1}{\pi} \int_0^\infty \langle \mathbf{u} \cdot \mathbf{u}' \rangle kr \sin(kr)\, \mathrm{d}r, \tag{2.1}$$

where k is the wavenumber and $r = | \mathbf{r} | = | \mathbf{x}' - \mathbf{x} |$. Expanding (2.1) for small k yields

$$E(k \to 0) = \frac{Lk^2}{4\pi^2} + \frac{Ik^4}{24\pi^2} + \cdots \tag{2.2}$$

provided, of course, that $\langle \mathbf{u} \cdot \mathbf{u}' \rangle$ decays sufficiently rapidly with separation for the expansion to be valid. (This requires that, at large r, $\langle \mathbf{u} \cdot \mathbf{u}' \rangle \sim O(r^{-6})$, or smaller.) The prefactors L and I are the integrals

$$L = \int \langle \mathbf{u} \cdot \mathbf{u}' \rangle \, \mathrm{d}\mathbf{r} \tag{2.3}$$

and

$$I = -\int r^2 \langle \mathbf{u} \cdot \mathbf{u}' \rangle \, \mathrm{d}\mathbf{r}, \tag{2.4}$$

which are known as the Saffman and Loitsyansky integrals respectively.

This suggests that, as far as the behaviour of the large scales is concerned, there are two important cases: when L is non-zero we have $E(k \to 0) \sim Lk^2$, which is called a Saffman spectrum, and in those cases where $L = 0$, we obtain $E(k \to 0) \sim Ik^4$, which is sometimes known as a Batchelor spectrum. These two canonical cases are usually referred to as Saffman and Batchelor turbulence, respectively, and we shall adopt this convention here. Other possibilities exist, however, such as $E(k \to 0) \sim k^p$, $p < 4$, but we shall postpone our discussion of these until § 2.2.

Both $E \sim Lk^2$ and $E \sim Ik^4$ spectra may be generated in computer simulations (see e.g. Ishida *et al.* 2006). Which type of turbulence is seen is determined by the initial conditions. A more interesting and controversial question, however, is whether grid turbulence is of the Saffman or Batchelor type. Until now, the experimental data have been ambiguous on this point, and so there is no uniformity of opinion on this issue. It is not even clear that all forms of grid turbulence must be of the same class. It is quite possible, for example, that different types of grids or different ranges of Re could produce different classes of turbulence.

Let us now consider Saffman turbulence in more detail. Noting that $\langle \mathbf{u}\cdot\mathbf{u}'\rangle$ is related to the longitudinal correlation function $f(r)$ by

$$\langle \mathbf{u}\cdot\mathbf{u}'\rangle = \frac{u^2}{r^2}\frac{\partial}{\partial r}(r^3 f), \tag{2.5}$$

it is clear that Saffman's integral can be rewritten as

$$L = 4\pi u^2 [r^3 f]_\infty, \tag{2.6}$$

where the subscript ∞ indicates $r \to \infty$. Thus a finite value of L implies an algebraic decline in f, as $f_\infty \sim r^{-3}$, though this does not exclude the possibility that $\langle \mathbf{u}\cdot\mathbf{u}'\rangle_\infty$ decays more rapidly, say exponentially. Indeed, it is not difficult to construct fields of isotropic turbulence in which $f_\infty \sim r^{-3}$, yet $\langle \mathbf{u}\cdot\mathbf{u}'\rangle_\infty$ falls off as a Gaussian (Davidson 2004).

Next, noting that ensemble and volume averages are equivalent, we have

$$L = \frac{1}{V}\left\langle \left[\int_V \mathbf{u}\,\mathrm{d}V\right]^2 \right\rangle, \tag{2.7}$$

where V is some large control volume. This gives us a simple physical interpretation of Saffmans integral as a measure of the amount of linear momentum held in the turbulence. It also provides a way of quantifying when we will, or will not, obtain a Saffman spectrum: we obtain such a spectrum whenever the turbulence contains a sufficiently large amount of linear momentum, $\boldsymbol{P} = \int_V \mathbf{u}\,\mathrm{d}V$. In particular, we require that $\langle \boldsymbol{P}^2\rangle$ grows with V as $\langle \boldsymbol{P}^2\rangle \sim V$ such that L remains finite and non-zero as $V \to \infty$ (Saffman 1967). If $\langle \boldsymbol{P}^2\rangle$ grows more slowly with V, then we obtain a Batchelor spectrum.

Saffman showed that L is an invariant of freely decaying turbulence. This follows from integrating the Kármán–Howarth equation,

$$\frac{\partial}{\partial t}\langle \mathbf{u}\cdot\mathbf{u}'\rangle = \frac{1}{r^2}\frac{\partial}{\partial r}\frac{1}{r}\frac{\partial}{\partial r}(r^4 u^3 K) + 2\nu\nabla^2\langle \mathbf{u}\cdot\mathbf{u}'\rangle, \tag{2.8}$$

combined with the observation that the longitudinal triple correlation $u^3K(r) = \langle u_x^2(\mathbf{x})u_x(\mathbf{x}+r\hat{\mathbf{e}}_x)\rangle$ falls as

$$(u^3K(r))_\infty \sim r^{-4} + O(r^{-5}) \tag{2.9}$$

at large r (Batchelor & Proudman 1956). The physical interpretation of the conservation of L is given in Davidson (2004, p. 360), where it is shown that the linear momentum in some large control volume V is approximately conserved in the sense that the flux of linear momentum out through the bounding surface is too small to change $\langle \boldsymbol{P}^2\rangle/V$ in the limit of $V \to \infty$.

One of the important consequences of the conservation of L is that it controls the rate of decay of energy. The argument goes as follows. Self-similarity of the large

scales demands

$$L = a_2 u^2 \ell^3, \tag{2.10}$$

where a_2 is a dimensionless constant, and so the integral scales are constrained to satisfy

$$u^2 \ell^3 = constant, \tag{2.11}$$

which is the hallmark of Saffman turbulence. (Although $E(k \to 0) \sim Lk^2$ is the definition of Saffman turbulence, the low-k form of E is very difficult to measure experimentally, whereas its hallmark, $u^2\ell^3 = constant$ is testable. Hence (2.11) is often taken as the test of Saffman turbulence.)

This is important as it may be combined with the empirical, but well established, relationship

$$\frac{\mathrm{d}u^2}{\mathrm{d}t} = -A\frac{u^3}{\ell}, \quad A = constant, \tag{2.12}$$

to give the decay laws

$$\frac{u^2}{u_0^2} = \left[1 + \frac{5}{6}A\frac{u_0 t}{\ell_0}\right]^{-6/5}, \tag{2.13}$$

$$\frac{\ell}{\ell_0} = \left[1 + \frac{5}{6}A\frac{u_0 t}{\ell_0}\right]^{2/5}, \tag{2.14}$$

where u_0 and ℓ_0 are the values of u and ℓ at $t = 0$ (Saffman 1967). (We shall address in § 2.4 the possibility that A could be a weak function of t in grid turbulence, if not in strictly homogeneous turbulence.)

Let us now consider Batchelor turbulence in which we have the spectrum, $E \sim Ik^4$. The first point to note is that it is the initial conditions which dictate whether we have a Saffman or Batchelor spectrum. That is, L is an invariant, and so if L is non-zero at $t = 0$ we have $E \sim Lk^2$ for all time, whereas $L = 0$ at $t = 0$ precludes such a spectrum. Note also that, unlike L, the integral I is not, in general, an invariant. That is, the Kármán–Howarth equation (2.8) integrates to give

$$\frac{\mathrm{d}I}{\mathrm{d}t} = 8\pi\,[u^3 r^4 K]_\infty \tag{2.15}$$

and we expect that the long-range pressure forces will, in general, establish long-range triple correlations of the form $K_\infty \sim cr^{-4}$, where c is some prefactor whose magnitude cannot be predicted in a rigorous way (Batchelor & Proudman 1956). Interestingly, though, simulations performed in very large computational domains show $I \approx constant$ once the turbulence has become fully developed (Ishida *et al.* 2006). This suggests that the prefactor $c = (r^4 K)_\infty$ is extremely small in mature turbulence. One of the consequences of the observed conservation of I is that one recovers Kolmogorovs decay laws in these simulations, i.e.

$$u^2 \sim t^{-10/7}, \quad \ell \sim t^{2/7}. \tag{2.16}$$

These decay laws rest on the assumption that I is conserved and they may be derived by combining (2.12) with the fact that self-similarity of the large scales yields

$$I = a_4 u^2 \ell^5 = constant, \tag{2.17}$$

for some dimensionless constant a_4. Evidently, (2.16) are the analogues of (2.13) and (2.14) for $E \sim Ik^4$ turbulence. Indeed, one of the recurring themes of isotropic

turbulence has been whether grid turbulence should be governed by (2.13) and (2.14) or else by (2.16). However, as we now show, these are not the only possibilities.

2.2. *Other decay laws*

Expansion (2.2) is valid only if $\langle \mathbf{u}\cdot\mathbf{u}'\rangle$ decays sufficiently rapidly with separation r. Let us suppose that, at $t = 0$, we (somehow) enforce long-range power-law correlations of the form

$$u^2 f_\infty = C_m r^{-m}, \tag{2.18}$$

where the C_m are dimensional prefactors. Then the Kármán–Howarth equation, combined with $K_\infty \sim cr^{-4}$, tells us that the coefficients C_m are invariants, provided that $m < 6$. So we shall restrict ourselves to $m < 6$, with $m = 3$ corresponding to a Saffman spectrum where, from (2.6), we have $C_3 = L/4\pi$. Note that the invariance of C_m, for $m < 6$, means that these long-range correlations cannot emerge spontaneously as a result of the turbulence dynamics; they have to be enforced at $t = 0$ as an initial condition. This, in turn, raises questions as to what is a physically acceptable initial condition, an issue to which we will return. Note also that an algebraic decay in $\langle \mathbf{u}\cdot\mathbf{u}'\rangle$ means that certain moments of the two-point correlations diverge, and so we should expect non-analytic behaviour of the spectral tensor at $\boldsymbol{k} = 0$.

Now self-similarity of the large scales demands $C_m = b_m u^2 \ell^m$ where the b_m are dimensionless constants. It follows that

$$u^2 \ell^m = constant, \quad m < 6, \tag{2.19}$$

which may be combined with (2.12) to give

$$\frac{u^2}{u_0^2} = \left[1 + \frac{m+2}{2m} A \frac{u_0 t}{\ell_0}\right]^{-2m/(m+2)}, \quad m < 6, \tag{2.20}$$

where u_0 and ℓ_0 are the values of u and ℓ at $t = 0$. (In grid turbulence $t = 0$ in (2.20) would correspond to the point where the turbulence first becomes fully developed.) Note that we recover Saffman's decay law for $m = 3$. It is interesting to compare (2.20) with the form of u^2 usually adopted when analysing grid turbulence data, i.e.

$$u^2 = C[t - \tau]^{-n}, \tag{2.21}$$

where τ is some virtual origin in time, $t = 0$ is now taken to correspond to the grid, and C is a dimensional constant.

Finally, we note that the energy spectrum corresponding to (2.18) takes the form

$$E(k \to 0) \sim k^{m-1}, m < 6, \tag{2.22}$$

with or without a log correction.

2.3. *A lower bound on the energy decay exponent (assuming A is constant)*

There now arises the interesting question of whether or not there is a lower bound on m, and hence on the energy decay exponent

$$n = \frac{2m}{m+2} \tag{2.23}$$

In this respect it is interesting to note that $m < 3$ causes Saffman's integral to diverge, and this seems unlikely for the following reason. We have seen that

$$L = \frac{1}{V}\left\langle \left[\int_V \mathbf{u}\,\mathrm{d}V\right]^2 \right\rangle, \tag{2.24}$$

where V is some large volume embedded within the turbulence. Thus we obtain a finite value of L if, and only if, on average, the turbulence contains just the right amount of linear momentum in a large control volume V, $\boldsymbol{P} = \int_V \mathbf{u}\,\mathrm{d}V$. That is, if L is to remain finite as $V \to \infty$, then $\langle \boldsymbol{P}^2 \rangle$ must grow with V as $\langle \boldsymbol{P}^2 \rangle \sim V$. If L diverges, on the other hand, then $\langle \boldsymbol{P}^2 \rangle$ must grow faster than $\langle \boldsymbol{P}^2 \rangle \sim V$. This is important as it is possible to use the central limit theorem to show that a growth faster than $\langle \boldsymbol{P}^2 \rangle \sim V$ is unlikely to occur, the implication being that m cannot be smaller than 3.

This can be seen from the following argument, suggested by Davidson (2004, p. 356). Let us take our control volume V to be a large sphere of radius R, large in the sense that $R \gg \ell$. We may consider the turbulence to be composed of a random sea of eddies (blobs of vorticity), each of which has some linear impulse, $2\mathbf{L}_i = \int \mathbf{x} \times \boldsymbol{\omega}\,\mathrm{d}V$. (Here the subscript i indicates the ith eddy within the volume V and $\boldsymbol{\omega}$ is vorticity.) Now, the linear momentum within some large spherical volume V is proportional to the sum of the linear impulses of the individual eddies contained within V, i.e. $\boldsymbol{P} \sim \sum \mathbf{L}_i$. Suppose that there are N eddies within V, each assigned a random value of $\mathbf{L}_i$ taken from a p.d.f. of zero mean. Then the central limit theorem requires that $\langle \boldsymbol{P}^2 \rangle \sim V$, which is consistent with a finite value of L in the limit of $V \to \infty$.

There is, however, a weakness in this argument. It turns out that the value of $\boldsymbol{P} = \int_V \mathbf{u}\,\mathrm{d}V$ depends not just on the vortices inside V, but also on the vortices external to V. This deficiency is readily accounted for, however, by using the more detailed analysis of Davidson (2009), and it turns out that the central finding remains unchanged.

In summary, then, the central limit theorem suggests that $\langle \boldsymbol{P}^2 \rangle$ can grow no faster than $\langle \boldsymbol{P}^2 \rangle \sim V$ and this requires Saffmans integral to be convergent. If this is indeed the case then the minimum value of m is $m = 3$, and the corresponding minimum decay exponent, assuming A is constant, is the Saffman value of $n = 6/5 = 1.2$.

2.4. *The influence of a temporal variation in A*

So far we have assumed that the coefficient A in (2.12) is constant. In practice, however, because of the streamwise variation in u^2/U^2 in grid turbulence, or else the slow decline of Re_λ, the coefficient A may exhibit some slight temporal variation (see § 1). This, in turn, changes the energy decay exponent. We close this section by considering the consequences of this slow variation in A. In the interests of brevity, we shall restrict the discussion to Saffman turbulence, where $u^2\ell^3 = constant$, though the results may be generalized in an obvious way to other cases. We focus on Saffman turbulence because, as we have seen, this yields the minimum decay exponent, and we are interested in how a temporal variation in A can influence this minimum exponent. Integrating

$$\frac{\mathrm{d}u^2}{\mathrm{d}t} = -A(t)\frac{u^3}{\ell}\,, \tag{2.25}$$

subject to $u^2\ell^3 = constant$, yields

$$\frac{u^2}{u_0^2} = \left[1 + \frac{5}{6}\frac{u_0}{\ell_0}\int_0^t A\,\mathrm{d}t\right]^{-6/5} \tag{2.26}$$

and

$$\frac{\ell}{\ell_0} = \left[1 + \frac{5}{6}\frac{u_0}{\ell_0}\int_0^t A\,\mathrm{d}t\right]^{2/5}, \tag{2.27}$$

where ℓ_0 and u_0 are the initial values of ℓ and u. Note that, as before, $t = 0$ in (2.26) and (2.27) correspond to the time where the turbulence first becomes fully developed.

The question now arises as to the form of $A(t)$. It is tempting to assume that $A(t)$ is a power law, analogous to (2.21), i.e. $u^2 = C[t-\tau]^{-n}$. However, there are no theoretical reasons why $A(t)$ should take this form. Nevertheless, we shall see that the experimental data suggests that A is a weak function of t, and that a reasonable approximation to $A(t)$ is

$$A(t) = C^*[t-\tau]^{-p}, \tag{2.28}$$

where C^* is another constant, $p \ll 1$, and τ is the same virtual origin as in (2.21). It is convenient to adopt this approximation to $A(t)$ as it allows us to parameterize the influence of a slow temporal decline of A on the energy decay exponent n.

Reverting the notation of § 2.1, we see that (2.28) takes the form

$$A(t) = A_0\left[1 + \frac{5}{6}\frac{A_0}{1-p}\frac{u_0 t}{\ell_0}\right]^{-p}. \tag{2.29}$$

More importantly, (2.26) and (2.27) now simplify to

$$\frac{u^2}{u_0^2} = \left[1 + \frac{5}{6}\frac{A_0}{1-p}\frac{u_0 t}{\ell_0}\right]^{-6(1-p)/5} \tag{2.30}$$

and

$$\frac{\ell}{\ell_0} = \left[1 + \frac{5}{6}\frac{A_0}{1-p}\frac{u_0 t}{\ell_0}\right]^{2(1-p)/5} \tag{2.31}$$

Note that (2.29) and (2.30) are consistent with (1.9), i.e. $A \sim [\langle \boldsymbol{u}^2\rangle]^{(5/6)p/(1-p)}$, which was derived on the basis of dimensional analysis. Note also that, for $p = 0$, we recover the classic decay laws of Saffman (1967). In summary, then, if $A(t)$ evolves slowly according to (2.28), and the experiments suggest this is a good approximation, then the minimum energy decay exponent (i.e. the decay exponent for Saffman turbulence) changes from $n = 1.2$ to $n = 1.2(1-p)$.

We shall see that experimental evidence shows that p is a small positive number of the order of $p \sim 0.08$. Clearly, the net effect of a slow variation in $A(t)$ is to reduce the energy decay exponent to a value slightly below that of the theoretical estimate of 6/5. We shall return to this issue in § 4.4.

3. Experimental details

The experiments were performed in the large recirculating wind tunnel of the Department of Energy and Process Engineering at The Norwegian University of Science and Technology, Trondheim, Norway. The tunnel test section is 2.7 m wide and 1.8 m high at the start of the test section, with an adjustable roof to compensate for the sidewall boundary layers. The test section is 11 m long.

The grid was produced from 2 mm sheet metal. Square holes 30 mm × 30 mm were punched at 40 mm spacing, giving a solidity of 44 % and a mesh size of $M = 40$ mm. The tests were performed at a grid Reynolds number of $Re_M = MU/\nu = 3.6 \times 10^4$.

Measurements were taken using a combination of two component laser Doppler anemometer (LDA) and one and two component hot-wire anemometry. The LDA system consisted of a 400 mW Spectra Physics air cooled argon laser mated to a Dantec Dynamics 60 mm fibre optics probe with a 40 MHz Bragg cell. Data evaluation was performed using a burst analyser and the data was weighted using the transit time option. Smoke was injected in the return section of the tunnel. The amount of smoke and the setting of the photo multiplier was adjusted so that the data rate was steady at about 3 kHz. Normally 10^5 samples were acquired per measurement position.

Purpose made probes were made for the hot-wire measurements by etching Wollaston wires with a 2.5 μm platinum–10 % rhodium core to a nominal length of 0.5 mm. This gave a wire length to Kolmogorov length scale ratio ranging from about $l_w/\eta \approx 2.6$ at the first measurement station to $l_w/\eta \approx 0.8$ at the most downstream position. For the X-wire probes 0.9 mm long 5 μm wires were used with wire angles close to $\pm 45^{\circ}$ and wire separation of 0.8 mm. The hot wires were operated at an overheat temperature of about 320°C using in-house made anemometers. The frequency response of the anemometers were adjusted to be better than $f = 30$ kHz at the test velocity of $U \approx 13.5\,\mathrm{m\,s^{-1}}$.

The signal from the anemometer was amplified so that the mean voltage spanned as much as possible of the ± 10 V range of the data acquisition system and sampled to a PC at 12 bit resolution to derive the mean velocity. The signal was then passed through a Krohn-Hite AC-coupled amplifier and low-pass filter unit. The high-pass filter of this unit is fixed at 0.1 Hz. The gain of this amplifier was continuously adjusted so that the turbulent signal fell within the ± 10 V range of the data acquisition system, giving an extra 10–40 times signal gain to improve the resolution. This conditioned signal was also sampled at 12 bit resolution on a separate PC to give high-resolution turbulence data.

After a number of tests at various x/M positions along the tunnel axis with filter cutoff settings of $f_c \approx 30$ kHz and sampling rates of $f_s \approx 60$ kHz, the pre-multiplied dissipation spectra were computed and inspected. For the following measurements sixth-order Butterworth filters were used and the cutoff frequency was set where the dissipation spectrum showed a minimum at the high frequency end, i.e. where the electronic noise started to drown the small-scale part of the signal. Typically f_c was 10 kHz close to the grid and 3.5 kHz at $x/M = 250$.

For most measurements 8×10^5 data were sampled per channel, but occasionally batches of up to 16×10^6 samples were acquired to assure statistical convergence for high-order moments.

4. Results

4.1. *Flow homogeneity and isotropy*

In the following, angle brackets $\langle \sim \rangle$ will be used to denote time averages, which, in the light of the ergodic hypothesis, are equivalent to ensemble averages in a statistically steady flow.

Initially, the grid was mounted at the entrance to the test section. However, as observed in previous experiments (e.g. Comte-Bellot & Corrsin 1966, Lavoie *et al.* 2007) it was found that the streamwise normal stress, $\langle u^2 \rangle$ was significantly higher than the two spanwise components, $\langle v^2 \rangle$ and $\langle w^2 \rangle$, and that improvement in the isotropy could be obtained by placing the grid upstream of a contraction. Instead of fitting a secondary contraction downstream of the grid as was done by Comte-Bellot & Corrsin (1966) and Lavoie *et al.* (2007), the grid was moved upstream into the test section contraction to a position where the ratio of the grid to test section area was 1.48. This gave a grid which was 72 meshes wide and 55 meshes high. This is considerably more meshes than has been used in most previous grid experiments. We therefore expect that sidewall boundary layer effects should be quite small. The test section started at $x/M = 30.3$ downstream of the grid and this is the position of the first measurement station. The roof of the test section was carefully adjusted to eliminate any streamwise velocity gradient. From $x/M \approx 45$ to 250 the streamwise time averaged velocity U, based on LDA measurements was found to be constant to

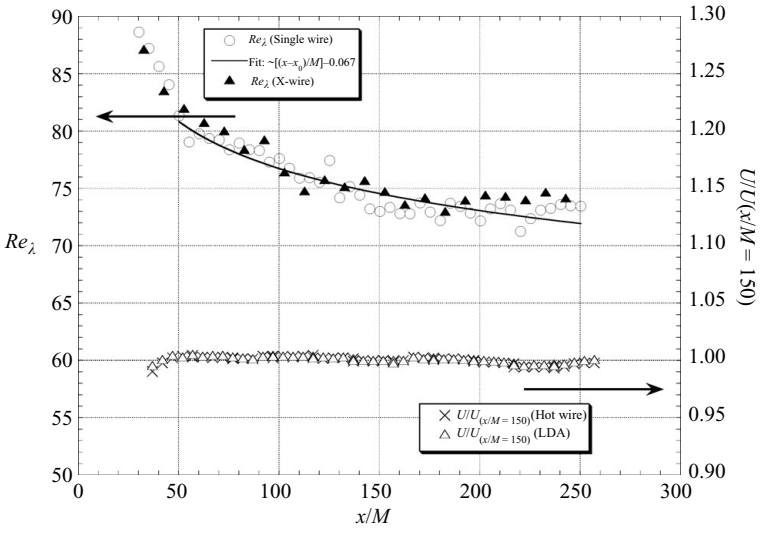

FIGURE 1. Streamwise distributions of Re_λ (left axis) and U (right axis).

within $-0.6\,\%/+0.3\,\%$ of the spatial mean and the two spanwise components, V and W, were found to be less than $-0.5\,\%/+1.1\,\%$ and $-0.4\,\%/+0.5\,\%$ of U, respectively.

Figure 1 shows the streamwise distribution of U, normalized with the value measured at $x/M = 150$. A weak acceleration downstream of the contraction exists on the centreline up to $x/M \approx 45$ and this affects the turbulent flow. This is illustrated by the development of the turbulent Reynolds number, $Re_\lambda = \lambda\sqrt{\langle u^2\rangle}/\nu$ (where λ is the Taylor microscale and ν the kinematic viscosity), which shows a much steeper decay rate in this region than further downstream, where $U \approx$ constant.

The spanwise homogeneity of the mean flow was also measured at a number of x/M positions. Except at the entrance to the test section ($x/M \approx 30$) where a small spanwise gradient was detected, U was uniform in the spanwise direction to within $\pm 0.3\,\%$. Figure 2 shows the spanwise distributions of the second-, third- and fourth-order moments of u. The spanwise uniformity is seen to be quite good for all moments. The turbulence intensity decays from about 2.75 % at the inlet of the test section to 0.8 % near the outlet while the skewness S_u is everywhere close to zero and the flatness F_u remains constant at about 2.95.

For isotropic turbulence the ratios $\langle u^2\rangle/\langle v^2\rangle$ and $\langle u^2\rangle/\langle w^2\rangle$ should be unity everywhere. The same applies to the ratio $\langle q^2\rangle/3\langle u^2\rangle = (\langle u^2\rangle + \langle w^2\rangle + \langle w^2\rangle)/3\langle u^2\rangle$, where $\langle q^2\rangle$ is twice the turbulent kinetic energy, i.e. $\langle q^2\rangle = \langle \mathbf{u}^2\rangle$. These quantities are shown in figure 3 where both LDA and hot-wire data have been included.

The ratio $\langle u^2\rangle/\langle v^2\rangle$ measured with LDA or hot wire are very close to 1 down to $x/M \approx 130$. Further downstream the trends from the two measurement techniques diverge, the LDA data show a steady increase while the ratio from the hot wires decreases slowly. The difference was traced back to inaccuracies in $\langle u^2\rangle$ measured by the LDA. The power-law decay, i.e. $\langle u^2\rangle \sim x^{-n}$, was well satisfied by all the hot-wire data (see §4.2), but for the LDA data the decay of $\langle u^2\rangle$ was found to slow down for $x/M > 130$ while $\langle v^2\rangle$ continued to follow the decay of the hot-wire data.

For the hot-wire data the ratio $\langle u^2\rangle/\langle v^2\rangle$ decreased slowly towards about 0.92 at the most downstream station indicating that the rate of decay was slightly slower for $\langle v^2\rangle$ than for $\langle u^2\rangle$. This trend is opposite to that observed for $\langle u^2\rangle/\langle w^2\rangle$. At the test

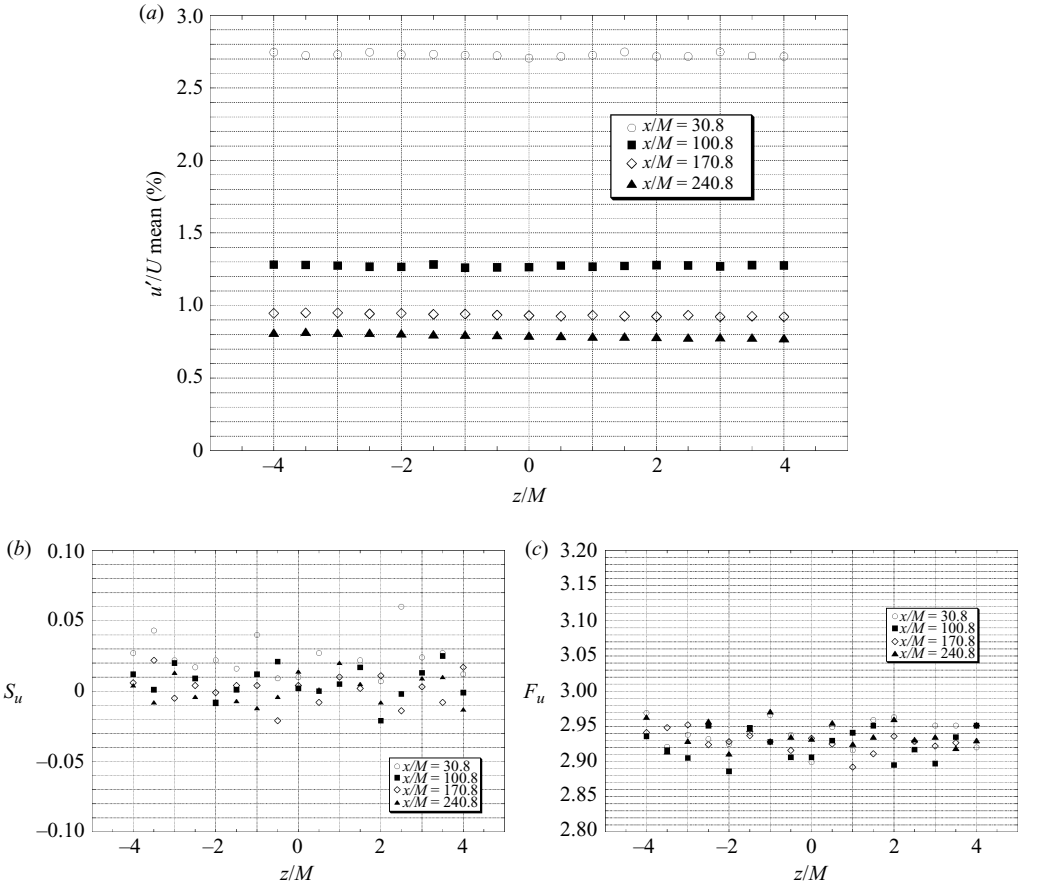

FIGURE 2. Spanwise distributions of $\langle u^2 \rangle$, skewness S_u and flatness F_u.

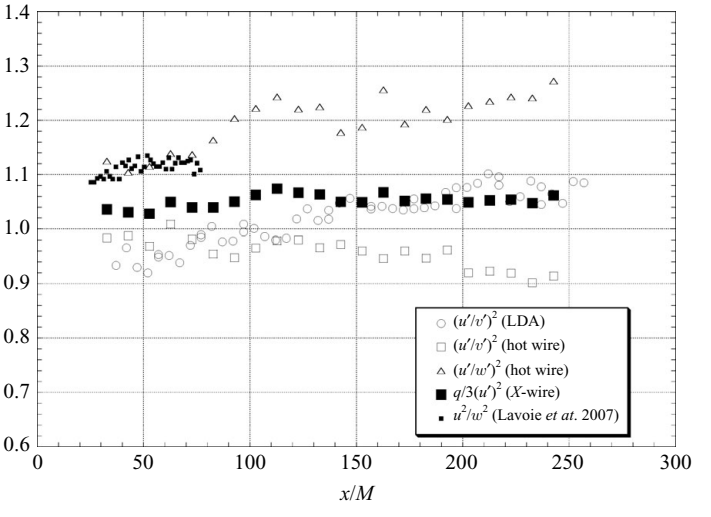

FIGURE 3. Streamwise distributions of stress ratios.

section entrance $\langle u^2\rangle/\langle w^2\rangle$ was measured to be about 1.1 and the ratio continued to increase downstream indicating a faster decay rate for $\langle w^2\rangle$ than for $\langle u^2\rangle$.

Even with a contraction downstream of the grid it is very difficult to get truly isotropic conditions. Using a contraction ratio of 1.36, Lavoie *et al.* (2007) also had problems obtaining isotropy in their square rod experiment. Their ratio $\langle u^2\rangle/\langle w^2\rangle$ is slightly higher than 1.1 and shows a development which is virtually identical to the present results (figure 3) in the overlapping x/M range. (Measurements of $\langle u^2\rangle/\langle v^2\rangle$ were not reported in the experiment of Lavoie *et al.*) Comte-Bellot & Corrsin (1966) typically obtained values of $\langle u^2\rangle/\langle v^2\rangle \approx 0.96$ in the range $20 < x/M < 300$ for their square rod grids which is not very different from the present values. (Again the ratio $\langle u^2\rangle/\langle w^2\rangle$ was not reported in their measurements.) Although a number of contraction ratios upstream of the test section were initially tried when setting up the present experiment, it was never possible to get both $\langle u^2\rangle/\langle v^2\rangle$ and $\langle u^2\rangle/\langle w^2\rangle$ to be 1 simultaneously over a significant streamwise distance. As the flow developed downstream $\langle u^2\rangle/\langle w^2\rangle$ was always found to increase steadily, showing that $\langle w^2\rangle$ decayed faster than $\langle u^2\rangle$. The reason for this remains unknown, but has been observed in many previous experiments, for example, in the experiment of Bennett & Corrsin (1978) and Lavoie *et al.* (2007).

Since true isotropy seems very difficult to achieve one may argue that instead of studying the decay rate of $\langle u^2\rangle$ it would make more sense to study the decay of $\langle q^2\rangle \sim x^{-n}$. Therefore $\langle q^2\rangle/3\langle u^2\rangle$ has also been included in figure 3. This ratio is seen to be virtually constant throughout the measurement range and although it is not identical to 1, the deviation is small and the scatter acceptable considering the extensive x/M range covered.

4.2. *Energy decay rate*

It has been shown repeatedly that it is very difficult to obtain reliable values from experimental data for the constants a, x_0 and n in the decay law

$$\frac{\langle u^2\rangle}{U^2} = a\left(\frac{x}{M} - \frac{x_0}{M}\right)^{-n}. \tag{4.1}$$

There are a number of reasons for this. The first point to note is that, comparing (4.1) with (2.20), and noting that $t = 0$ in (2.20) corresponds to the start of mature turbulence, we see that x_0 is not the point where the turbulence first becomes fully developed, but rather a distance $n\ell_0 A^{-1}(U/u_0)$ upstream of that point. So we do not know in advance where x_0 should be. Second, many investigations have covered a rather limited x/M range with only a small number of streamwise positions. In this case it may be difficult to determine exactly where the initial transient decay region ends and the fully developed turbulence begins. If data from the initial transient region are included in the fit, higher values of the decay exponent n are normally obtained. A third, related problem is that if the x/M range is too limited then the derived value of n becomes very sensitive to the choice of x_0. Typically x_0/M has been found to be of the order 5–10. If the x/M range investigated is only a few multiples longer than this, one finds that even small changes in the estimated x_0/M will severely affect the estimates of both a and n.

As the streamwise distance increases, the measurements start to be affected by noise. Some obvious sources are electronic noise generated or picked up by the anemometres and amplifier/filter units, low frequency oscillations from the wind tunnel fan control system and turbulence transmitted through the pressure field from the sidewall boundary layers. Some investigators (e.g. Bennett & Corrsin 1978) have

constructed correction schemes to account for these effects. However, instead of trying to correct the low turbulence intensity data we have chosen to do the measurements at such high streamwise resolution that the onset of departure from (4.1) due to noise will be evident in the data.

It is fair to assume that the initial development of the flow depends strongly on the initial conditions, as demonstrated by Lavoie *et al.* (2007). Kistler & Vrebalovich (1966) showed that the constant a in (4.1) is directly related to the pressure drop across the grid. Only the decay exponent n for fully developed turbulence can be assumed to be independent of the grid geometry. Instead of doing a direct power law fit to the data, (4.1) was rewritten as

$$\ln\left(\frac{\langle u^2\rangle}{U^2}\right) = \ln(a) - n\,\ln\left(\frac{x}{M} - \frac{x_0}{M}\right), \tag{4.2}$$

and a linear fit made.

Three fitting procedures were applied to the data to extract the best estimates for n.

4.2.1. *Regression method*

This method is based on the work by Mohamed & LaRue (1990) where we search for the fit that gives the smallest variance between the data and (4.2). If $f(x)$ is the function to be fitted to a set of data points $d_i(x_i)$, we search for the minimum of

$$\sigma^2 = \frac{1}{(N-1)}\sum_{i}^{N}(d_i(x_i) - f(x_i))^2 \ :$$

(*a*) Starting with all the available data a curvefit was made and the variance σ^2 recorded. The data for the most upstream x/M positions were then eliminated one-by-one from the fit until the lowest value of σ was found. This position, x_{low}, was then assumed to be the end of the initial decay range.

(*b*) Keeping x_{low}/M fixed the same procedure was used to eliminate data from the high end of the x/M measurement range. The x_{high}/M position where σ now had a minimum was taken to be the point where system noise was starting to affect the data or the final decay commenced. The values obtained for a, x_0 and n for this best fit was taken to be the correct values using this method.

Figure 4 shows Regression fits to one single wire data set and two X-wire sets for which all three normal stresses had been obtained using the same probe. Hence $\langle q^2\rangle$ could be calculated for both sets. Even though this set is considerably more elaborate to obtain than $\langle u^2\rangle$ used for the single wire data fit, the results are very similar. All sets showed that the fit should be limited to the region $45 < x/M < 200$. For $x/M > 200$ it is clear that the data starts to depart from the fits as noise begins to affect the data. The values obtained for the fit constants are shown in table 1.

With this method we find $1.11 \leqslant n \leqslant 1.15$, which is slightly below the theoretical minimum of Saffman's $n = 1.2$. However, we shall see shortly that A decays slowly in accordance with (2.28), which reduces n in a way which is consistent with the data.

4.2.2. *Local exponent method*

Since the single wire data was taken at intervals of $\Delta x/M = 2.5$ with a spatial resolution better than $\Delta s/\Delta x = 0.01$, it was expected that the local exponent could also be derived with reasonable accuracy using two-point differencing. Rewriting (4.2)

Method	Variable	Single wire $\langle u^2 \rangle$	X-wire Set1 $\langle q^2 \rangle$	X-wire Set2 $\langle q^2 \rangle$
Regression fit	x_0/M	7.3	5.5	4.5
	n	1.11	1.12	1.15
Local exponent	n	1.15	1.12	1.14
Maximum decay	n	1.12	1.18	1.21

TABLE 1. Constants obtained from the fit procedures.

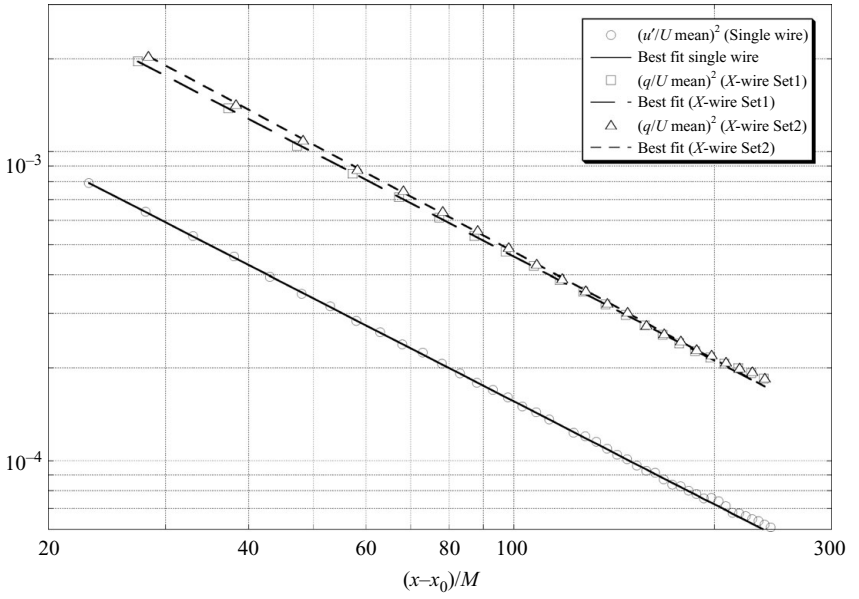

FIGURE 4. Fit to $\langle u^2 \rangle$ from a single wire data set and $\langle q^2 \rangle$ for two X-wire data sets.

the exponent at position $(x - x_0)/M$ may then be expressed as

$$n(x) = -\ln\left[\frac{\frac{\langle u^2\rangle}{U^2}(x - x_0 + \Delta x)}{\frac{\langle u^2\rangle}{U^2}(x - x_0 - \Delta x)}\right] \Big/ \ln\left[\frac{x - x_0 + \Delta x}{x - x_0 - \Delta x}\right].$$

Using the value for x_0 obtained from the Regression method, the local exponent could now be found (figure 5). Both the single wire and X-wire data show the same trends, but it is obvious that this method gives an estimated value for n which depends on position. For $50 < (x - x_0)/M < 175$ the values obtained are reasonably constant and fall between $n \approx 1.15$ and 1.20. Further downstream the local exponent decreases and the scatter increases. Even though the Regression method indicated that a good fit would be obtained for data up to $x/M = 200$, the Local exponent method indicates that the decay rate as described by (4.1) with a constant exponent should not be explored much beyond $x/M = 175$.

The exponents obtained by averaging the local values over the range $50 < x/M < 175$ are also given in table 1. These lie in the range $1.12 \leqslant n \leqslant 1.17$ and are very close to the values obtained by the previous method. Again, the measurements are consistent with Saffman turbulence in which $A(t)$ is slowly decreasing.

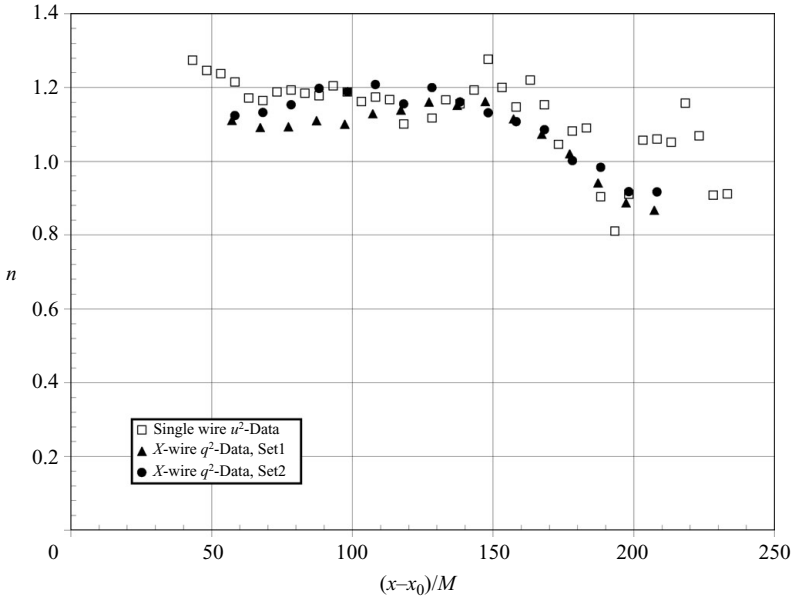

FIGURE 5. Local exponents of $\langle u^2 \rangle$ from one single wire data set and from $\langle q^2 \rangle$ for two X-wire data sets.

4.2.3. *Maximum decay range method*

Finally, we will apply the method of Lavoie *et al.* (2007). Fitting data to (4.1) implies that one tries to optimize three independent coefficients. The experience is that if the number of data points is low, many values for the constants may fit the data equally well. These authors claim that if one of these constants may be assumed to be known, the uncertainty of the remaining constants decreases by an order of magnitude. If, for example, x_o is kept constant and a power-law range really exists for a range of the data, the remaining constants obtained from the fit should remain the same for any subset that falls within this range. Hence by scanning different subsets in the measurement domain with fixed x_o, one searches for the value of x_o that gives constant values for a and n independent of which subset is used.

We have already found from the Regression method that the data for $x/M > 200$ is not likely to follow (4.1). Hence we will once again limit the range of the fit to $x/M < 200$ and starting from the full remaining set we will drop data used for the fit one-by-one from the low end of x/M. Figure 6 shows the exponents of the power-law decay range obtained when this method was applied to the single wire data as function of the assumed starting point, x_{start}/M and x_o/M. It is apparent from the figure that a value of $x_o/M \approx 6$ gives the longest range of constant n, which then is close to 1.12. x_o/M obtained in this way is not very different from the value obtained by the Regression method, and the estimated exponent is only marginally higher.

The method was also applied to $\langle q^2 \rangle$ from the two X-wire data sets. However, the correct combination of n and x_o/M was less well defined in this case because the region of constant n was significantly narrower than for $\langle u^2 \rangle$. This is probably due to the fact that two independent sets of measurements and three velocity components are required to obtain $\langle q^2 \rangle$, so the scatter in the data is significantly higher than for the single wire $\langle u^2 \rangle$ data. Tentative values are given in table 1.

Summing up the results from the three methods used to obtain the decay exponent, (but excluding the less reliable X-wire data using method 3), we find that n in

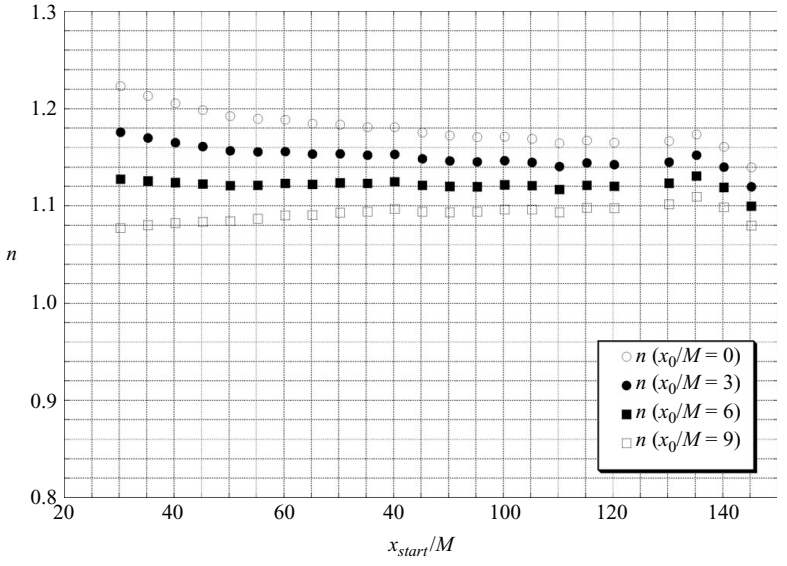

FIGURE 6. Decay exponent as function of starting coordinate. $\langle u^2 \rangle$ from a single wire data set.

this experiment was typically $n = 1.13$ with an uncertainty of ± 0.02. All of the measurements of n are close to, but slightly lower than, Saffman's exponent of $n = 1.2$.

4.3. *Higher order moments*

For isotropic turbulence we expect the skewness and flatness to be 0 and 3 respectively for all velocity components. For the homogeneous grid flow they are expected to be slightly, but not very different, due to the slow streamwise decay. The streamwise flux of kinetic energy to downstream regions of lower energy leads to a small positive velocity skewness. A close inspection of figure 7 shows that there is a very slow streamwise development in the skewness. According to the approximate model of Maxey (1987) the odd-order moments of the fluctuations may be written as

$$\frac{\langle u^{2p+1} \rangle}{\langle u^{2p} \rangle \langle u^2 \rangle^{1/2}} \approx pA \frac{\langle u^2 \rangle^{1/2}}{U}, \tag{4.3}$$

for $p \geqslant 1$. With $p = 1$, the skewnesses S_u, S_v and S_w should all be of the order of the turbulence level, $\langle u^2 \rangle^{1/2}/U$, which drops from about 0.03 at the first measurement station to slightly below 0.008 at the last location. This agrees well with the range measured for the skewnesses.

The flatness factors F_u, F_v and F_w are constant at about 2.93 throughout the flow. This suggests that the single point velocity statistics are very close to, but not quite, Gaussian. These measurements agree well with the data of Townsend (1947), who suggests that F_u lies between 2.9 and 3 while S_u should be zero.

4.4. *Length scales*

Irrespective of what the correct value for the decay exponent n is, the squared Taylor microscale must grow linearly with the distance from the grid for isotropic turbulence, provided $\langle u^2 \rangle$ decays as a power law. Defining the Taylor microscale as $\lambda^2 = \langle u^2 \rangle / \langle (\partial u/\partial x)^2 \rangle$, for isotropic turbulence this may be written as $\lambda^2 = 15\nu \langle u^2 \rangle / \epsilon =$

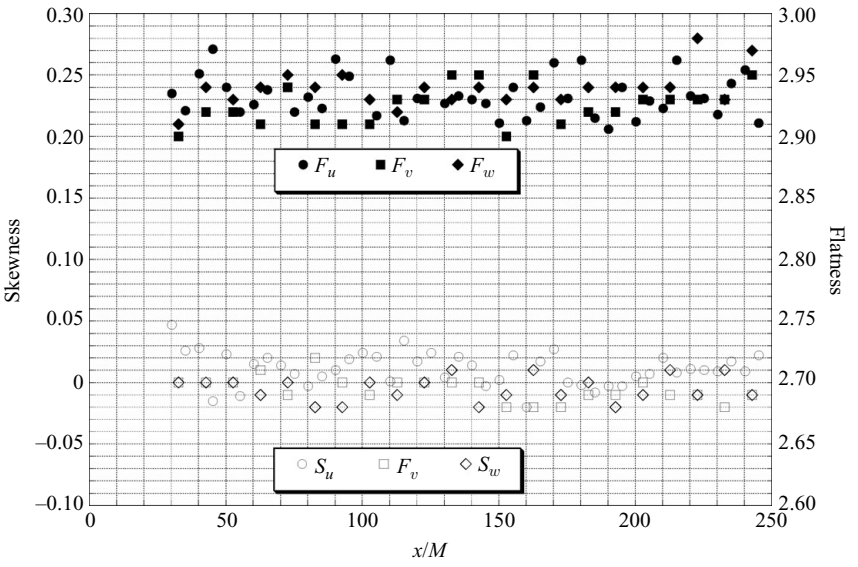

FIGURE 7. Skewness and flatness factors for u, v and w.

$5\nu\langle q^2\rangle/\epsilon$. Combined with the decay equation $(U/2)\mathrm{d}\langle q^2\rangle/\mathrm{d}x = -\epsilon$ it then follows that

$$\lambda^2 = \frac{-10\nu}{U}\frac{\langle q^2\rangle}{\mathrm{d}\langle q^2\rangle/\mathrm{d}x} = \frac{10n\nu}{U}(x - x_0) \tag{4.4}$$

without any assumptions about the decay exponent, n.

In order to determine the distribution of λ^2 it is necessary to determine as accurately as possible $\langle(\partial u/\partial x)^2\rangle$, or the dissipation rate ϵ. With the present data there are at least three options to determine $\langle(\partial u/\partial x)^2\rangle$ or ϵ. First, $\langle(\partial u/\partial x)^2\rangle$ may be computed directly from the time series. Linked with the isotropic relation $\epsilon = 15\nu\langle(\partial u/\partial x)^2\rangle$ the dissipation rate is obtained. This estimate will be denoted ϵ_{iso}. ϵ may also be obtained directly from the gradient of the $\langle q^2\rangle$ distribution as $\epsilon = -(U/2)\mathrm{d}\langle q^2\rangle/\mathrm{d}x$. We will denote this ϵ_{q2}. The third method relies on the universality of the spectral inertial subrange. Let $F_{11}(k_1)$ be the one-dimensional spectrum of u. Kolmogorov's five-third law, $F_{11}(k_1) = C_1\epsilon^{2/3}k_1^{-5/3}$ may then be used to extract an independent estimate for ϵ, although one-dimensional spectra at these kinds of Reynolds numbers do not exhibit a broad $-5/3$ range. In this experiment, ϵ_{spec} was extracted from the peak in the compensated spectrum ($k_1^{5/3}F_{11}(k_1) = C_1\epsilon^{2/3}$) with $C_1 = 0.5$ as recommended by Pearson, Krogstad & van de Water (2002). This estimate is labelled ϵ_{spec}.

The three estimates for the dissipation rate are shown in figure 8. The agreement between the methods is seen to be excellent and the choice of method is therefore not likely to affect the values obtained for λ^2 significantly. We have chosen to use the isotropic estimate ϵ_{iso}, since it appears to have the least scatter.

Also included in the figure is the dissipation rate that follows from the fit made to (4.1) for the measured $\langle u^2\rangle/U^2$. The expected decay of the dissipation rate may then be written as

$$\frac{M\epsilon}{U^3} = -\frac{3}{2}\frac{\mathrm{d}(\langle u^2\rangle/U^2)}{\mathrm{d}(x/M)} = \frac{3}{2}na\left(\frac{x - x_0}{M}\right)^{-n-1}. \tag{4.5}$$

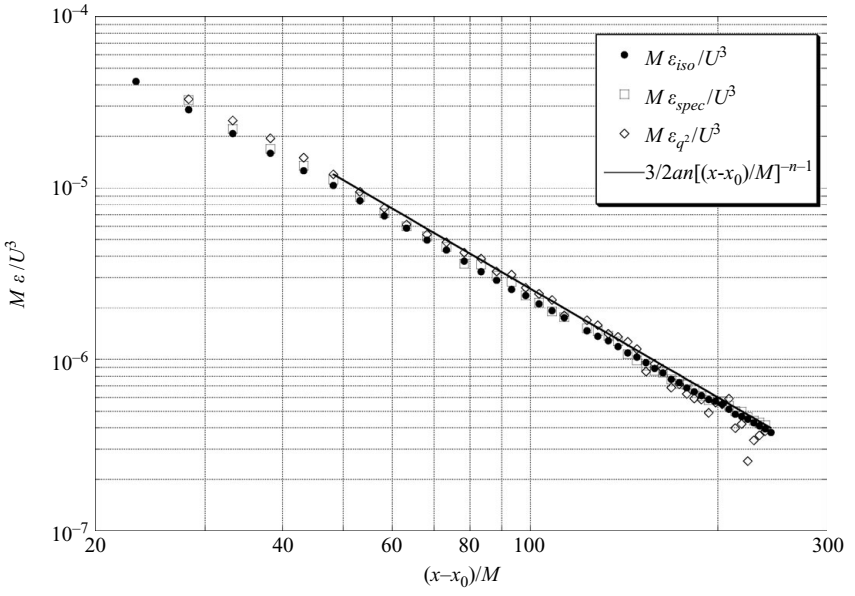

FIGURE 8. Estimates of dissipation rate using ϵ_{iso}, ϵ_{spec} and ϵ_{q2}.

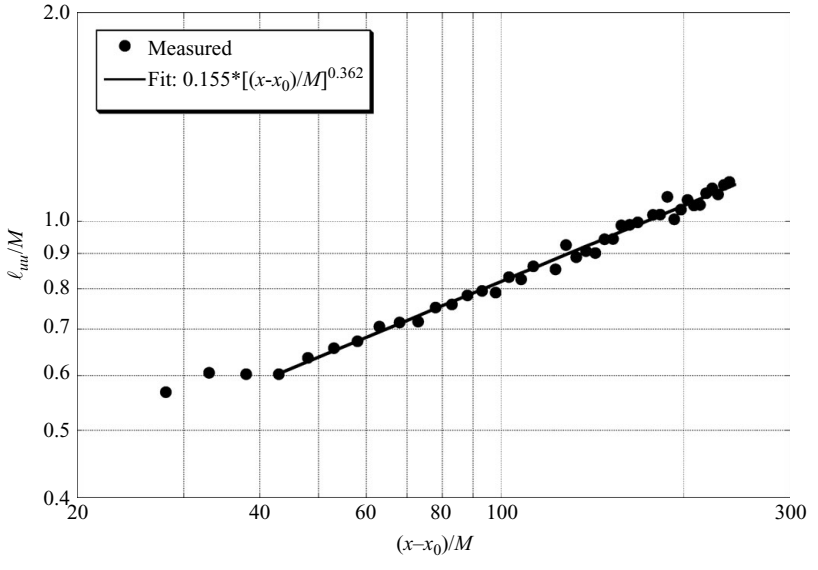

FIGURE 9. Development of the integral scale.

Using the exponent and the offset obtained in §4.2.1 this estimate is plotted for $45 < (x - x_0)/M < 200$, which is the range where the fit applies, and is seen to match the data well. This verifies that the data is internally consistent. (When the fit to $\langle q^2 \rangle / U^2$ was used it gave virtually indistinguishable estimates, so these have not been included in the plot.)

The development of $(\lambda/M)^2$ follows very closely the expected linear trend (figure 9). A best fit to the data in the range $45 < (x - x_0)/M < 200$, using x_0 as found from the energy decay power law fit, gave an exponent of 0.97. Given the experimental scatter, this may be taken as effectively unity.

Introducing (4.4) into the definition of $Re_\lambda = u\lambda/\nu$ we find that the Reynolds number should decay with x as

$$Re_\lambda = \sqrt{10na\frac{UM}{\nu}}\left(\frac{x-x_0}{M}\right)^{(1-n)/2}. \tag{4.6}$$

A curve fit to the measured Re_λ for $50 < x/M < 250$ using (4.6) (see figure 1) gave an exponent of $(1-n)/2 = 0.067$, which suggests a decay exponent of $n = 1.13$. This is the same as the mean exponent found in § 4.2, verifying that the data is self-consistent.

Next we investigate the development of the integral length scale ℓ_{uu}, which is defined as

$$\ell_{uu} = \int_0^\infty \frac{\langle u(x)u(x+r)\rangle}{\langle u^2\rangle}\,\mathrm{d}r. \tag{4.7}$$

Rather than measuring the correlation $\langle u(x)u(x+r)\rangle$ simultaneously at two streamwise positions in space, it was approximated by using the Taylor frozen equilibrium hypothesis, i.e. $u(x)u(x+r) \approx u(x)u(x-U\Delta t)$. Ideally the correlation should decay monotonically to zero for large r, but this is rarely found to be the case in experiments, where the correlation is found to oscillate slowly around 0 indefinitely. Therefore the integral in (4.7) was terminated at the first zero crossing. The integral scale is shown in figure 9 based on the single wire measurements. Although the data for ℓ_{uu} exhibits considerable more scatter than λ^2, it is obvious that it also increases downstream according to a power law. The data for $(x-x_0)/M < 50$ is seen to be affected by the small initial acceleration in U. This assumption is further supported by the Re_λ distribution shown in figure 1 and the single wire local decay exponents shown in figure 5, which tend to be higher than the rest for the first few stations. A fit to the ℓ_{uu}/M data in the range $50 < x/M < 200$ gave a growth exponent of $m = 0.362$ which is somewhat lower than the Saffman exponent of $m = 0.4$. However, it is consistent with (2.31) and hence Saffman turbulence, if we take a value of $p \approx 0.09$, which turns out to be close to the measured value of p (see next section).

4.5. *The variation of A and its influence on the power-law exponents for* $\langle u^2\rangle$ *and* ℓ_{uu}

We have already commented that the coefficient A in expression (2.12), which is related to the dissipation rate through

$$\epsilon = \frac{3}{2}Au^3/\ell_{uu}, \tag{4.8}$$

is not strictly a constant in grid turbulence. Figure 10 shows A calculated using the estimated values of ϵ_{iso} and ℓ_{uu}. Also shown is the best fit power law $A \sim [(x-x_0)/M]^{-p}$ where x_0 is the value obtained from § 4.2 and the data was again fitted in the range $50 < x/M < 200$. The best fit exponent is $p = 0.075$. From (2.30) we see that the corresponding energy decay exponent for Saffman turbulence is $n = 1.11$, which is consistent with the measured values of $n = 1.13 \pm 0.02$. The corresponding power-law exponent for ℓ_{uu}, on the other hand, is given by (2.31), and $p = 0.075$ would have $\ell_{uu} \sim t^{0.370}$, which is very close to the measured exponent of 0.362. This demonstrates that the exponents derived for $A(t)$, the energy decay and the growth rate of ℓ are all internally consistent, and also consistent with Saffman turbulence in which $u^2\ell_{uu}^3 = constant$. Table 2 summarizes the exponents found.

Finally, we return to (2.11), i.e. the question of whether the product $\langle u^2\rangle\ell_{uu}^3$, or indeed $\langle u^2\rangle\ell_{uu}^5$, is constant for grid generated turbulence. It is clear from figure 11 that $\langle u^2\rangle\ell_{uu}^5$ increases steadily with downstream distance, while the Saffman integral $L \sim \langle u^2\rangle\ell_{uu}^3$ remains constant for $(x-x_0)/M > 45$, within the experimental scatter. All

Exponent	n in $\langle u^2\rangle \sim t^{-n}$	m in $\ell_{uu} \sim t^{-m}$
Calculated assuming Saffman turbulence and $p = 0.075$	1.11	0.370
Measured	1.13 ± 0.02	0.362

TABLE 2. Comparison of power-law exponents.

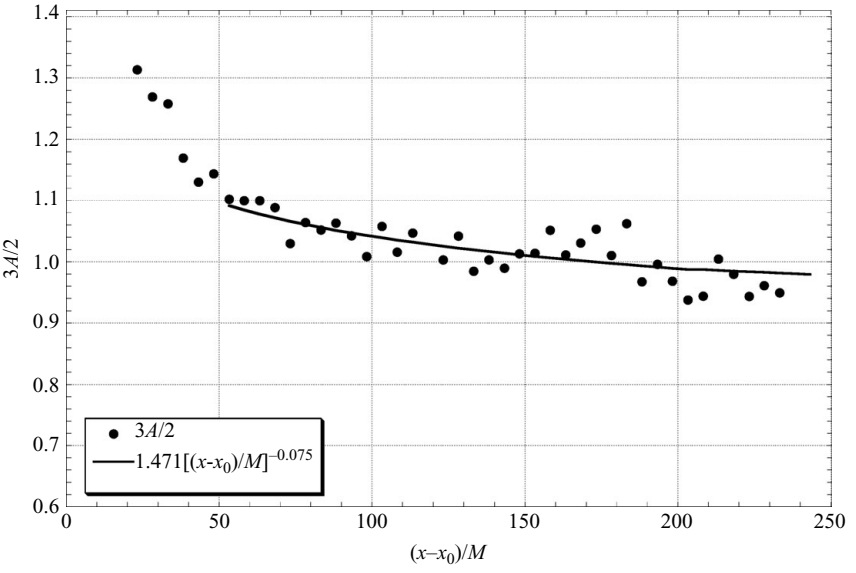

FIGURE 10. Development of A in (2.12).

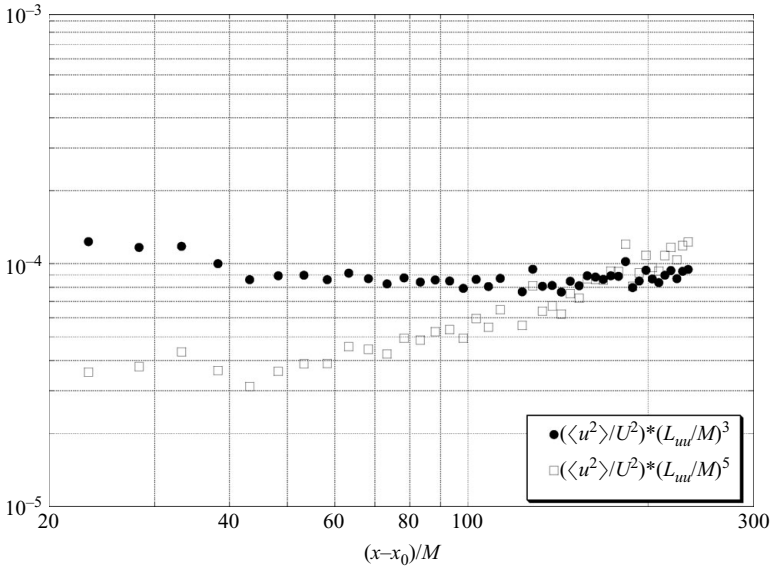

FIGURE 11. Developments of $\langle u^2\rangle \ell_{uu}^3$ and $\langle u^2\rangle \ell_{uu}^5$.

in all, the data for $(x - x_0)/M > 45$ is consistent with grid turbulence being Saffman turbulence, evolving in time with the modified expressions (2.30) and (2.31).

5. Conclusions

We have shown that, in strictly homogeneous turbulence in which $A = constant$, the minimum decay exponent in the scaling $u^2 \sim t^{-n}$ is the Saffman value of $n = 6/5$. However, in grid turbulence, A may vary slowly due to the weak streamwise inhomogenuity of the flow or else due to the decline in Re_λ with x, and indeed the experiments indicate $A \sim t^{-p}$, $0 < p \ll 1$. This slow decline in A changes the predicted decay exponent for Saffman turbulence to $n = 6(1 - p)/5$, which then represents the minimum decay exponent for weakly inhomogeneous grid turbulence, i.e. u^2 can decay no slower than $u^2 \sim t^{-1.2(1-p)}$. The corresponding predicted variation in the integral scale is $\ell \sim t^{0.4(1-p)}$. In any event, whether the turbulence is strictly homogeneous or weakly inhomogeneous, the hall-mark of Saffman turbulence is $u^2\ell^3 = constant$.

Our experiments show the following. Once the turbulence is fully developed and the streamwise acceleration falls to zero, which corresponds to $x > 50\,M$ in the present set-up, we find:

(i) $u^2\ell^3 \approx constant$;

(ii) $u^2 \sim t^{-n}$, $n = 1.13 \pm 0.02$;

(iii) $\ell \sim t^{0.362}$;

(iv) $A \sim t^{-p}$, $p = 0.075$.

Finding (i) is highly suggestive of Saffman turbulence. Moreover, given the measured value of p, Saffman turbulence would require $u^2 \sim t^{-1.11}$ and $\ell \sim t^{0.370}$, which are very close to the actual measurements. It is almost certain, therefore, that our turbulence is of the type envisaged by Saffman in 1967. It follows that, for a given value of p, the turbulence energy decays as slowly as it can do.

Perhaps some words of caution are appropriate at this point. Although it seems very likely that the turbulence behind our grid is Saffman turbulence, it is entirely possible that different grids, or different ranges of Re, could produce different results. As noted in § 2, whether or not L is finite, depends on how much linear impulse is imparted to the turbulence during its creation. If $\langle[\int_V \boldsymbol{u}\,\mathrm{d}V]^2\rangle$ is smaller than $O(V)$, then $L = 0$ and the turbulence will decay faster than $u^2 \sim t^{-1.2(1-p)}$. It seems plausible, for example, that the symmetric shedding of vortices from a square or round bar grid at low-to-moderate Re will result in little linear impulse, and hence $L = 0$ (Saffman 1967). On the other hand, the less organized shedding of vorticity from a conventional grid at high Re, or from our perforated plate grid, seems more likely to yield a finite value of L, which is what we have observed.

The authors would like to acknowledge the help from Dr Muyiwa Adaramola in setting up the experiment. Also, discussions with Mr Stuart Fox on the Regression method in the initial phase of this project proved very useful.

REFERENCES

Batchelor, G. K. & Proudman, I. 1956 The large-scale structure of homogeneous turbulence. *Phil. Trans. R. Soc.* A **248**, 369–405.

Bennett, J. C. & Corrsin, S. 1978 Small Reynolds number nearly isotropic turbulence in a straight duct and a contraction. *Phys. Fluids* **21**, 2129–2140.

Comte-Bellot, G. & Corrsin, S. 1966 The use of a contraction to improve the isotropy of grid-generated turbulence. *J. Fluid Mech.* **25**, 657–682.

Davidson, P. A. 2004 *Turbulence, An Introduction for Scientists and Engineers.* Oxford University Press.

Davidson, P. A. 2009 On the role of angular momentum conservation in homogenous turbulence. *J. Fluid Mech.* **632**, 329–358.

Ishida, T., Davidson, P. A. & Kaneda, Y. 2006 On the decay of isotropic turbulence. *J. Fluid Mech.* **564**, 455–475.

Kistler, A. L. & Vrebalovich, T. 1966 Grid turbulence at large Reynolds numbers. *J. Fluid Mech.* **26**, 37–47.

Lavoie, P., Djenedi, L. & Antonia, R. A. 2007 Effects of initial conditions in decaying turbulence generated by passive grids. *J. Fluid Mech.* **585**, 395–420.

Maxey, M. R. 1987 The velocity skewness measured in grid turbulence. *Phys. Fluids* **30**, 935–938.

Mohamed, M. S. & LaRue, J. C. 1990 The decay power law in grid-generated turbulence. *J. Fluid Mech.* **219**, 195–214.

Pearson, B. R., Krogstad, P.-Å. & van de Water, W. 2002 Measurements of the turbulent energy dissipation rate. *Phys. Fluids* **14**, 1288–1290.

Pullin, D. I. & Saffman, P. J. 1998 Vortex dynamics in turbulence. *Annu. Rev. Fluid Mech.* **30**, 31–51.

Saffman, P. J. 1967 The large-scale structure of homogeneous turbulence. *J. Fluid Mech.* **27**, 581–593.

Townsend, A. A. 1947 The measurement of double and triple correlation derivatives inisotropic turbulence. *Proc. Cam. Phil. Soc.* **43**, 560–572.

Warhaft, Z. & Lumley, J. L. 1978 An experimental study of the decay of temperature fluctuations in grid generated turbulence. *J. Fluid Mech.* **88**, 659–684.